Electronic Supplementary Information(ESI)

A critical role of catalyst morphology in low temperature synthesis of carbon nanotube–transition metal oxide nanocomposite

Xiaoyan Jin,[a] Joohyun Lim,[a] Yoonhoo Ha,[b] Nam Hee Kwon,[a] Hyeyoung Shin,[b] In Young Kim,[a] Nam-Suk Lee,[c] Myung Hwa Kim,[a] Hyungjun Kim,[b,*] and Seong-Ju Hwang[a,*]

[a] Department of Chemistry and Nanoscience, College of Natural Sciences, Ewha Womans University, Seoul 03760, Republic of Korea

[b] Graduate School of Energy, Environment, Water, and Sustainability (EEWS), Korea Advanced Institute of Science and Technology (KAIST), Daejeon 34141, Republic of Korea

[c] National Institute for Nanomaterials Technology (NINT), Pohang University of Science and Technology (POSTECH), Pohang 37673, Republic of Korea

Fig. S1 Top view of the *p*(2×1) surface unit cell. Possible binding sites on the bare MnO (100) surface are denoted by filled dots; 2 atop (green) and 3 bridge sites (orange). After DFT geometry optimization, the binding energies of carbon atom are shown in table by the side of the unit cell. Among them, atop Mn site provides the most favorable binding site for C atom.

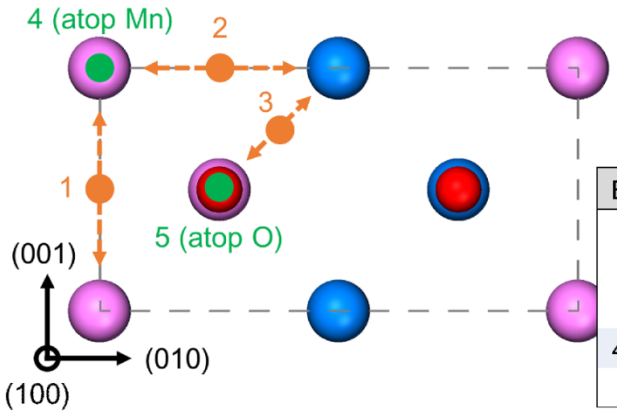

Binding site	$E_{b,C}$ (eV)
1	-5.76
2	-4.47
3	-4.47
4 (atop Mn)	**-7.34**
5 (atop O)	No binding

$$E_{b,nC} = E_{MnO@nC} - (E_{MnO} + 0.5n(E_{C2H2}-E_{H2}))$$

Fig. S2 Field emission-scanning electron microscopy (FE-SEM) images of (a) MnO precursors and (b) their products from the reaction with C_2H_2, (c) high resolution-transmission electron microscopy (HR-TEM) images of MnO precursors subjected to the reaction with C_2H_2, and (d) powder X-ray diffraction (XRD) patterns of (i) MnO precursors and (ii) their products from the reaction with C_2H_2.

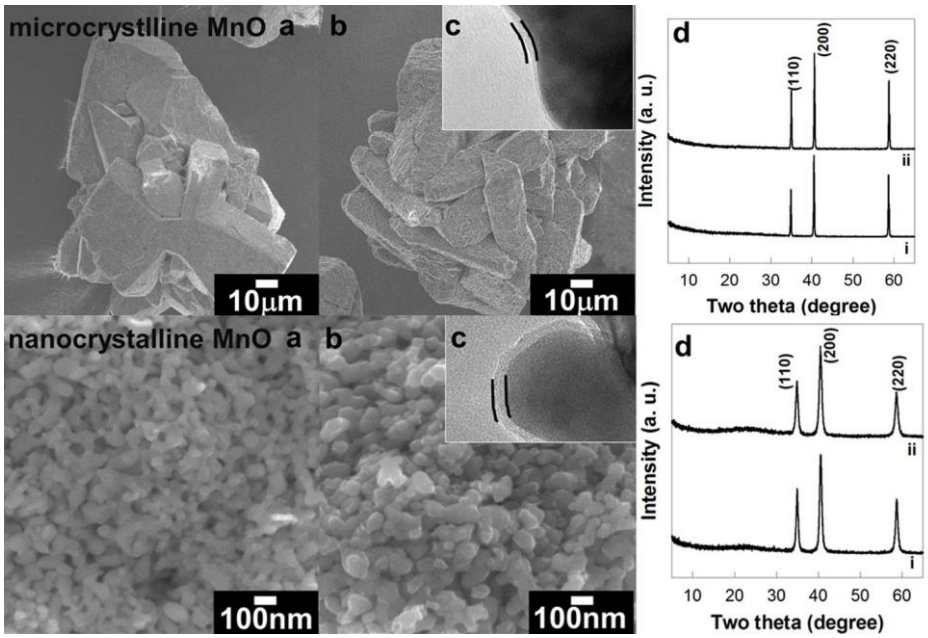

Fig. S3 (a) FE-SEM image and (b) powder XRD pattern of layered MnO_2 nanosheet after the reaction of C_2H_2 vapor at 400 °C. According to powder XRD analysis, the formation of partially reduced Mn_3O_4 phase is attributable to the weaker reducing power of C_2H_2 at a lower temperature.

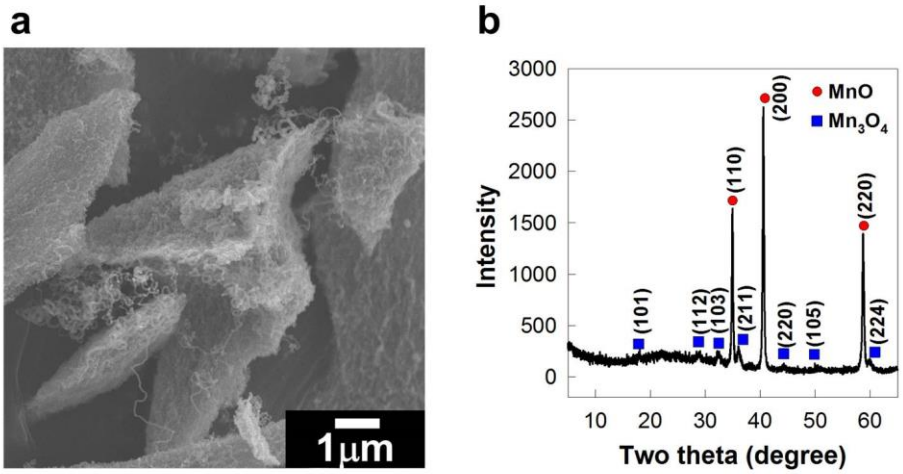

Fig. S4 FE-SEM images of layered TiO_2 nanosheet (a) before and (b) after the reaction with C_2H_2 and (c) XRD data of layered TiO_2 nanosheet (i) before and (ii) after the reaction with C_2H_2. According to the XRD analysis, the layered TiO_2 nanosheet experiences a phase transition from lepidocrocite-type structure to anatase TiO_2 one.

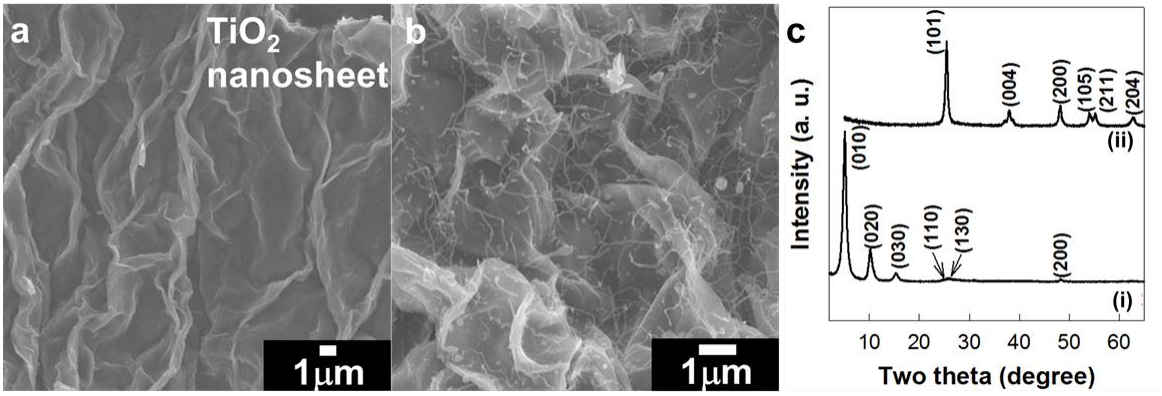

Fig. S5 (a) HR-TEM image and (b) energy dispersive spectrometry (EDS)–elemental mapping data of carbon nanotube (CNT) obtained from the acidic etching of the CNT–MnO nanocomposite. The EDS–elemental mapping analysis demonstrates that the MnO catalyst is completely removed by acidic etching.

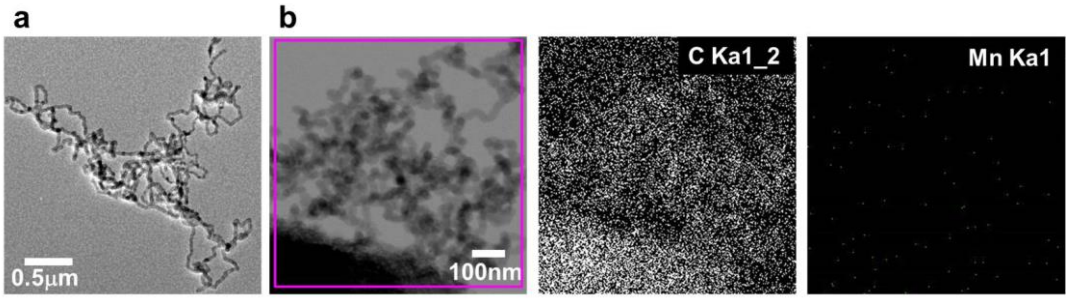

Fig. S6 Energy-filtered transmission electron microscopy (EFTEM)–elemental mapping data of the CNT–MnO nanocomposites at (a) 0 and (b) 20 h.

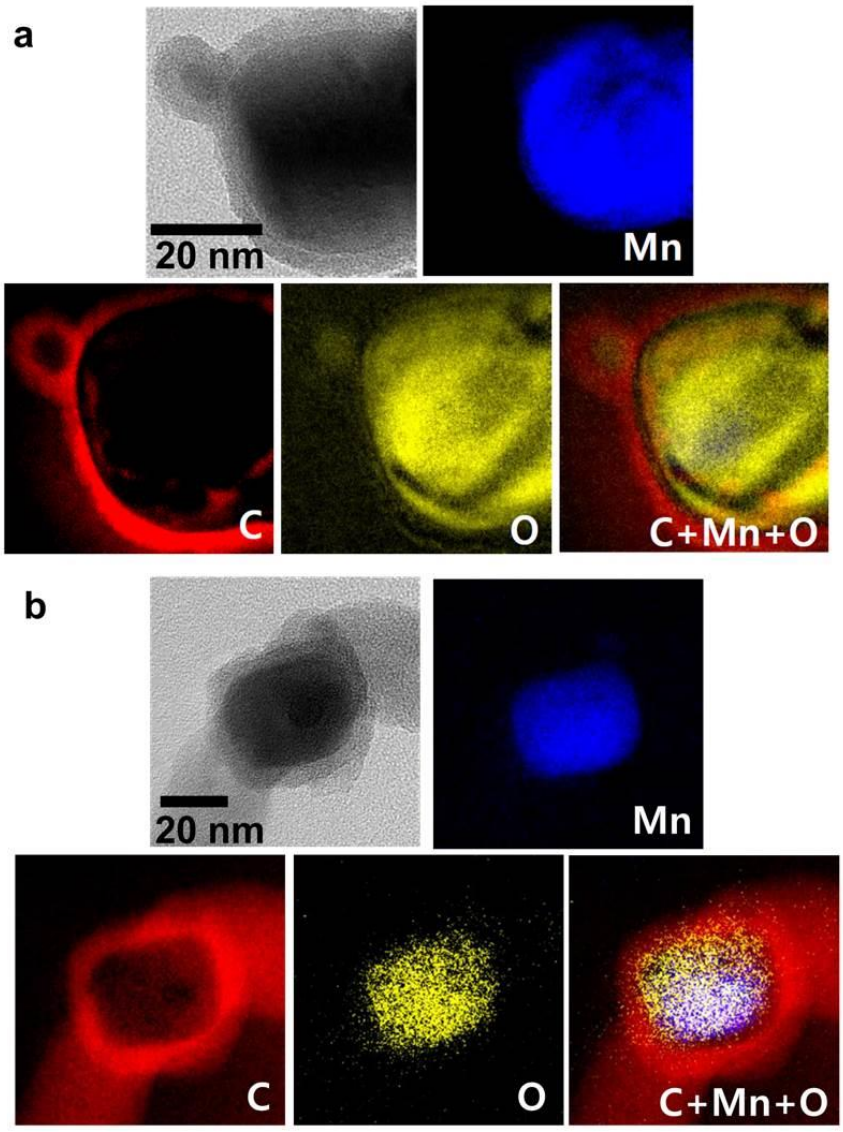

Fig. S7 HR-TEM images of CNT from the CNT–MnO nanocomposite.

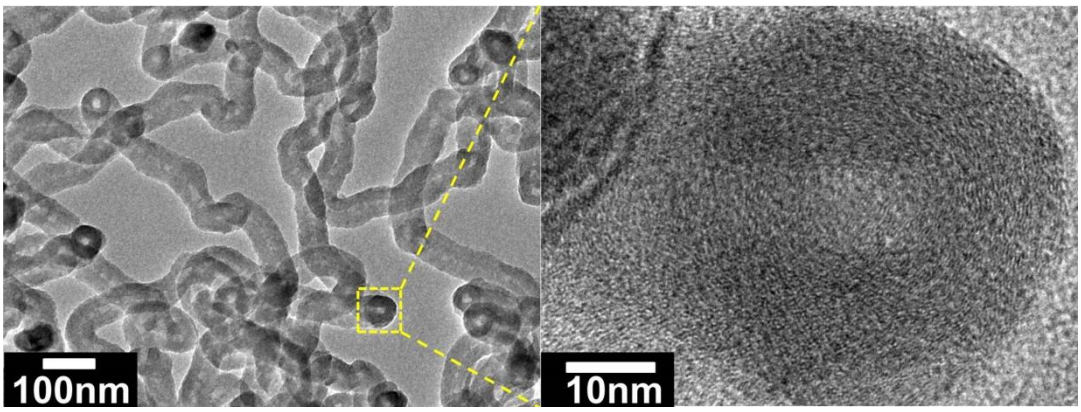

Fig. S8 Powder XRD patterns of (a) the precursor layered MnO_2 nanosheet and the CNT–MnO nanocomposites of (b) **MC1**, (c) **MC2**, (d) **MC3**, and (e) **MC4**.

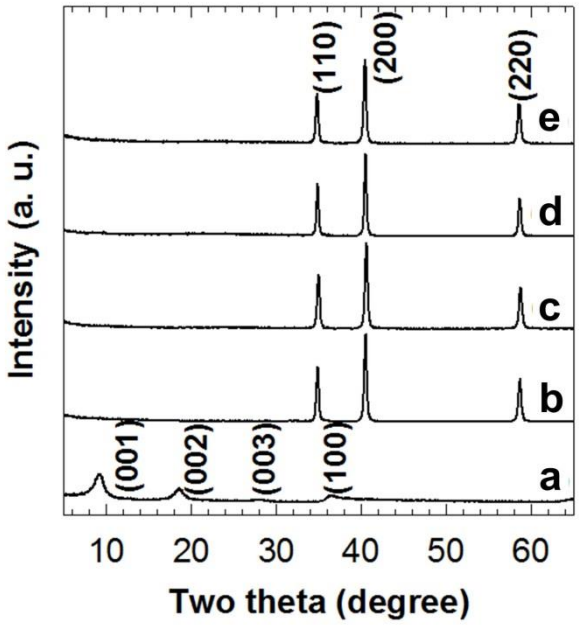

Table S1 Relative proportions of carbon species in the CNT–MnO nanocomposites determined from micro-Raman results.

	MC1	**MC4**
D peak	45.7%	42.5%
G peak	20.0%	21.7%
functional group	22.7%	27.5%
amorphous carbon	11.6%	8.3%
Total	100.0%	100.0%

Fig. S9 Coulombic efficiency of the CNT–MnO nanocomposites of **MC1** (green), **MC2** (blue), **MC3** (red), **MC4** (pink), and the precursor layered MnO_2 nanosheet (black) at a current density of 100 mA g^{-1}.

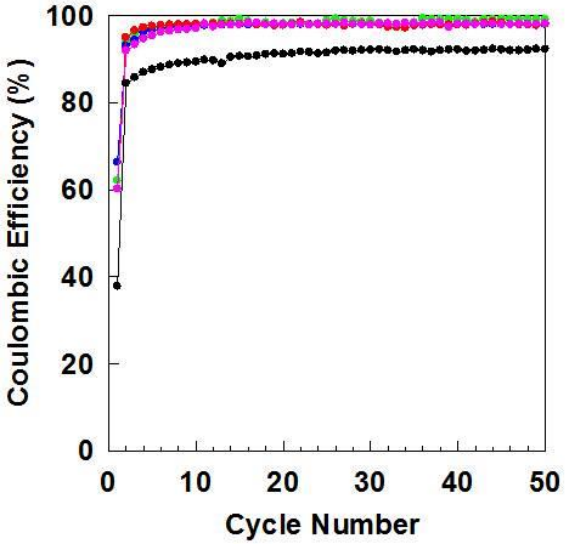

Fig. S10 Potential profiles of the **MC2** nanocomposite at current density of 100 mA g^{-1}.

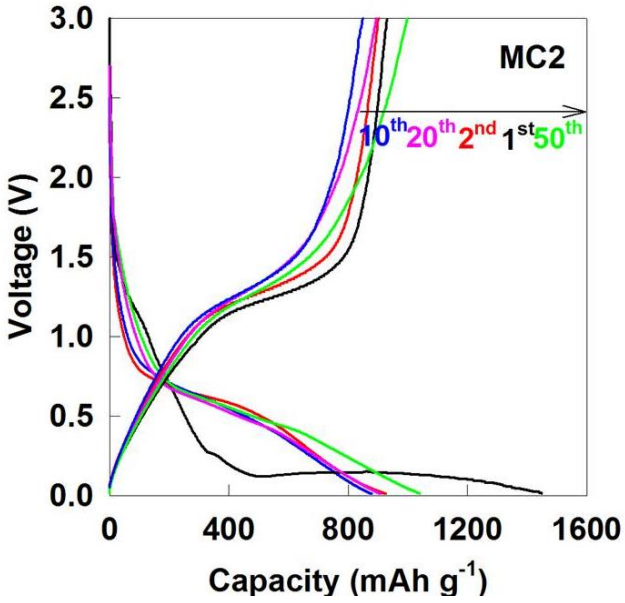

Fig. S11 Schematic illustration of the growth mechanism of CNT.

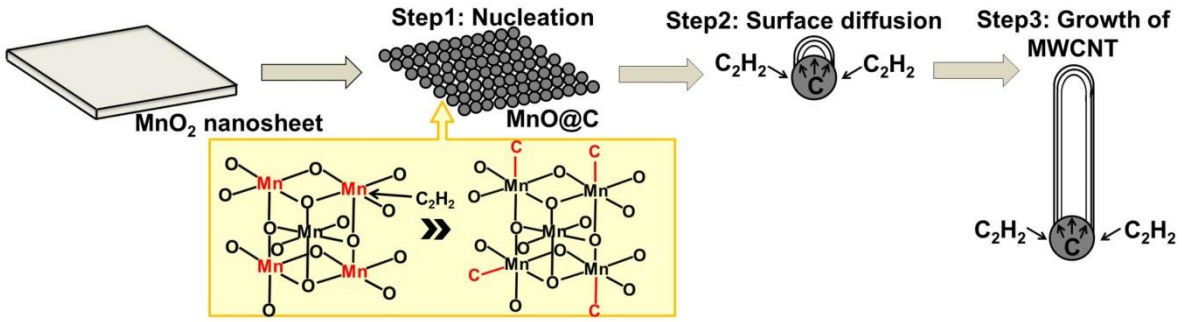

Fig. S12 p(2×1) unit cell of MnO, containing 8 Mn atoms; four Mn atoms with spin-up (pink, denoted as +) and the other Mn atoms with spin-down (blue, denoted as -), along with 8 O atoms. Colored plane represents dipole interaction between opposite spin-oriented (111) layers in the antiferromagnetic-II ordered MnO.

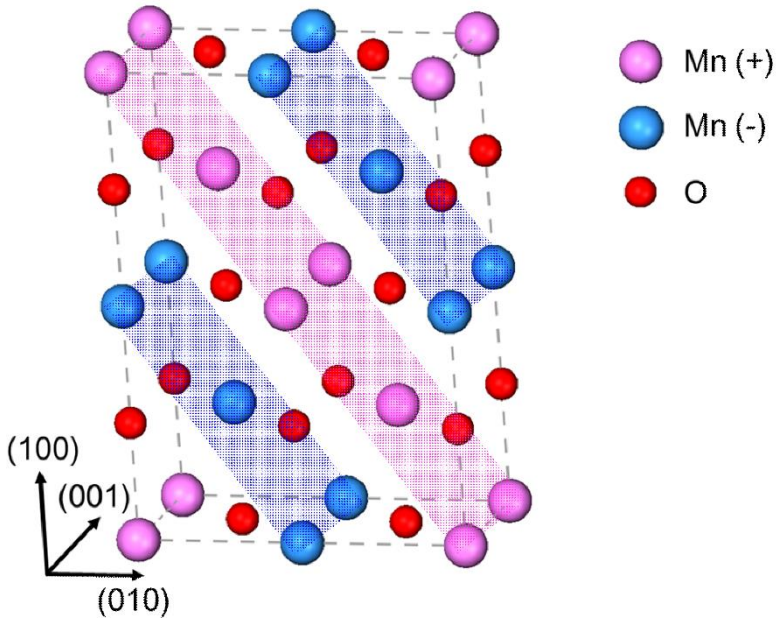

Fig. S13 (a) FE-SEM image, (b) powder XRD pattern, and (c) XPS spectra of Fe-substituted MnO_2 nanosheet subjected to C_2H_2 treatment at 400 °C. No observation of zero-valent Fe-related signals in the XRD and XPS data underscores that Fe-substituted manganese oxides are responsible for the efficient growth of CNT.